Expanding the Temperature Range of Biomimetic Synthesis Using a Ferritin from the Hyperthermophile *Pyrococcus furiosus*

Mackenzie J. Parker,[†,‡,§] Mark A. Allen,[†,‡,§] Brad Ramsay,[†,‡,§] Michael T. Klem,[†,‡,§] Mark Young,[*,‡,§,||] and Trevor Douglas[*,†,‡,§]

Department of Chemistry and Biochemistry, Department of Plant Sciences and Plant Pathology, Center for Bio-Inspired Nanomaterials, and Thermal Biology Institute, Montana State University, Bozeman, Montana 59717

Received September 24, 2007. Revised Manuscript Received October 29, 2007

Biological macromolecules, such as protein cages and viruses, have been shown to serve as excellent templates for the synthesis of nanoscale particles of inorganic materials that give rise to homogeneous properties. However, a limitation in using these molecules in these synthetic reactions has been the temperature stability of the biological template. It is hypothesized that the use of thermally stable proteins isolated from hyperthermophilic bacteria and archaea will overcome this limitation and expand the list of materials with interesting properties that are amenable to biomimetic synthesis. This study reports the synthesis of maghemite (γ-Fe_2O_3) at elevated temperatures using a ferritin with extraordinary temperature stability from the hyperthermophilic archaeon *Pyrococcus furiosus*. Protein−mineral composites were characterized by dynamic light scattering, size exclusion chromatography, and transmission electron microscopy, which confirmed the successful encapsulation of the iron oxide particle in the interior of the ferritin. Magnetic characterization revealed saturation of the γ-Fe_2O_3 nanoparticles at significantly lower field strengths than previously seen with mammalian ferritin−mineral composites. The observed behavior suggests the formation of well ordered, single domain particles within the archaeal ferritin. Electrostatic surface comparisons of the interior surface of human, horse spleen, and *P. furiosus* ferritins revealed a significant difference in the charge density between the mammalian and archaeal proteins which may influence the crystal structure of the material formed. These results demonstrate the utility of temperature stable protein cages as templates in the syntheses of desirable inorganic nanomaterials.

Introduction

Biomineralization, the formation of solids in biological systems, has provided the inspiration for the controlled formation of a range of novel inorganic materials.[1–12] In biomineralization, self-organization of organic based templates provides a scaffolding for the assembly of inorganic materials.[9,13,14] For example, the iron storage protein ferritin naturally self-assembles into a hollow cage-like architecture that acts to direct the mineralization of iron oxides *in vivo*, sequestering excess iron ions in the soluble protein container and preventing the iron dependent radical-producing reactions that are lethal to the cell.[15–17] Such activity can also be utilized *in vitro* in the synthesis of materials with novel or interesting magnetic,[18–20] catalytic,[21] or semiconducting properties.[22,23] Ferritins have been used as templates in the synthesis of magnetite nanoparticles for potential magnetic resonance imaging (MRI) applications[24] and of CdSe and

* Corresponding authors. E-mail: myoung@montana.edu (M.Y.) or tdouglas@chemistry.montana.edu (T.D.).
† Department of Chemistry and Biochemistry.
‡ Center for Bio-Inspired Nanomaterials.
§ Thermal Biology Institute.
|| Department of Plant Science and Plant Pathology.

(1) Ensign, D.; Young, M.; Douglas, T. *Inorg. Chem.* **2004**, *43*, 3441.
(2) Klem, M. T.; Willits, D.; Solis, D. J.; Belcher, A. M.; Young, M.; Douglas, T. *Adv. Funct. Mater.* **2005**, *15*, 1489.
(3) Wong, K. K. W.; Mann, S. *Adv. Mater.* **1996**, *8*, 928.
(4) Ueno, T.; Suzuki, M.; Goto, T.; Matsumoto, T.; Nagayama, K.; Watanabe, Y. *Angew. Chem., Int. Ed.* **2004**, *43*, 2527.
(5) Meldrum, F. C.; Douglas, T.; Levi, S.; Arosio, P.; Mann, S. *J. Inorg. Biochem.* **1995**, *58*, 59.
(6) Mackle, P.; Charnock, J. M.; Garner, C. D.; Meldrum, F. C.; Mann, S. *J. Am. Chem. Soc.* **1993**, *115*, 8471.
(7) Nam, K. T.; Kim, D. W.; Yoo, P. J.; Chiang, C. Y.; Meethong, N.; Hammond, P. T.; Chiang, Y. M.; Belcher, A. M. *Science* **2006**, *312*, 885.
(8) Chiang, C. Y.; Mello, C. M.; Gu, J.; Silva, E. C. C.; van Vliet, K. J.; Belcher, A. M. *Adv. Mater.* **2007**, *19*, 826.
(9) Kramer, R. M.; Li, C.; Carter, D. C.; Stone, M. O.; Naik, R. R. *J. Am. Chem. Soc.* **2004**, *126*, 13282.
(10) Yang, S.; Ford, J.; Ruengruglikit, C.; Huang, Q. R.; Aizenberg, J. *J. Mater. Chem.* **2005**, *15*, 4200.
(11) Yang, S.; Chen, G.; Megens, M.; Ullal, C. K.; Han, Y. J.; Rapaport, R.; Thomas, E. L.; Aizenberg, J. *Adv. Mater.* **2005**, *17*, 435.
(12) Hall, S. R. *Adv. Mater.* **2006**, *18*, 487.
(13) Mann, S. *Nature* **1991**, *349*, 285.
(14) Mann, S. *Nature* **1993**, *365*, 499.
(15) Hentze, M. W.; Muckenthaler, M. U.; Andrews, N. C. *Cell* **2004**, *117*, 285.
(16) Harrison, P. M.; Arosio, P. *Biochim. Biophys. Acta* **1996**, *1275*, 161.
(17) Theil, E. C. *Annu. Rev. Biochem.* **1987**, *56*, 289.
(18) Klem, M. T.; Young, M.; Douglas, T. *Mater. Today* **2005**, *8*, 28.
(19) Mayes, E. L.; Bewick, A.; Gleeson, D.; Hoinville, J.; Jones, R.; Kasyutich, O. I.; Nartowski, A.; Warne, B.; Wiggins, J. A. L.; Wong, K. K. W. *IEEE Trans. Magn.* **2003**, *39*, 624.
(20) Warne, B.; Kasyutich, O. I.; Mayes, E. L.; Wiggins, J. A. L.; Wong, K. K. W. *IEEE Trans. Magn.* **2000**, *36*, 3009.
(21) Bell, A. T. *Science* **2003**, *299*, 1688.
(22) Mao, C. B.; Solis, D. J.; Reiss, B. D.; Kottmann, S. T.; Sweeney, R. Y.; Hayhurst, A.; Georgiou, G.; Iverson, B.; Belcher, A. M. *Science* **2004**, *303*, 213.
(23) Duan, X.; Chunming, N.; Sahi, V.; Chen, J.; Parce, W.; Empedocles, S.; Goldman, J. L. *Nature* **2003**, *425*, 274.
(24) Uchida, M.; Flenniken, M. L.; Allen, M. A.; Willits, D. A.; Crowley, B. E.; Brumfield, S.; Willis, A. F.; Jackiw, L.; Jutila, M.; Young, M. J.; Douglas, T. *J. Am. Chem. Soc.* **2006**, *128*, 16626.

10.1021/cm702732x CCC: $40.75
Published on Web 01/15/2008

ZnSe nanoparticles for potential quantum dot applications.[25–27] Other protein cages, such as viruses, also assemble from individual subunits into well-defined architectures and can be used for the size dependent synthesis of non-native nanomaterials.[28–30] Viral particles, devoid of their nucleic acids, such as Cowpea chlorotic mottle virus have been used in the syntheses of iron oxide and polyoxometalate nanoparticles or as a scaffolding for the assembly of composite materials.[28,29,31] The bacteriophage M13 has been genetically engineered to produce peptides that, through a screening process, can be selected for the ability to specifically direct the synthesis of a variety of materials, such as Au or Au−Co_3O_4 nanowires, to serve as electrodes for the development of small flexible Li-ion batteries,[7] magnetic CoPt/FePt nanowires, or ZnSe filaments.[8,22,32] These biomimetic syntheses are possible as a result of the complementary interactions between the organic protein template and the synthetic inorganic materials.

While biological macromolecules are responsible for the synthesis of several materials that are necessary for life, their use in material synthesis is often limited by their relatively low thermal stability compared with other synthetic methods. Many nanomaterial products require synthesis temperatures higher than most proteins can tolerate.[33–36] Isolation of the protein templates from the thermophilic and hyperthermophilic organisms may be one approach to ease this limitation. The recent isolation of a number of thermally stable protein cages, such as ferritins,[37,38] heat shock proteins (Hsp),[39,40] and DNA-binding proteins from stressed cells,[41,42] from hyperthermophilic archaea significantly expands the temperature range of *in vivo* biomineralization and the potential for high temperature *in vitro* biomimetic syntheses. A small heat shock protein (sHsp) from *Methanococcus jannaschii*, reported to be stable to 70 °C, has been used to synthesize $L1_0$ CoPt nanoparticles with novel magnetic properties and platinum nanoparticles for the biocatalytic production of H_2.[2,43] These illustrate the use of thermally stable proteins as templates for materials synthesis at elevated temperatures. As the number of protein cages isolated from hyperthermophilic organisms increases so too will the variety and size of the materials that can be synthesized using a biomimetic approach.

Recently, a ferritin was isolated from *Pyrococcus furiosus*, a marine anaerobe that lives in thermal springs where temperatures can reach 120 °C.[37] The protein was cloned from its native host and was found to be easily overexpressed in *Escherichia coli*.[37] The recombinant *Pyrococcus* ferritin (PfFn) was subjected to incubation at temperatures up to 120 °C and was shown to retain the iron sequestering capabilities for over 0.5 h at these extremely high temperatures.[37] The structure of this protein has been solved to 2.75 Å and has been shown to be homologous to other ferritins from different taxa.[44,45] The temperature stability of this protein opens up the possibility for syntheses of inorganic materials at temperatures previously unattainable with other biomolecular templates.

This study reports the use of PfFn in the biomimetic synthesis of maghemite (γ-Fe_2O_3) nanoparticles at elevated temperatures. This material was selected because (1) magnetic iron oxide particles have potential applications in MR imaging, cancer treatment, and memory storage and (2) the material has been previously synthesized and characterized magnetically with mammalian ferritin templates; thus, data is available for comparison. The PfFn templated syntheses were performed at 65 and 85 °C with two theoretical loading factors of 1000 Fe/cage or 2000 Fe/cage. The reactions attempted at temperatures higher than 85 °C resulted in bulk iron oxide formation. The PfFn−mineral composites were characterized, and their magnetic properties were compared to previously synthesized γ-Fe_2O_3 particles in mammalian ferritins. The results show that PfFn can successfully template these particles, which show enhanced magnetic properties previously unobserved in other ferritin−γ-Fe_2O_3 composites.

Experimental Section

Details on cloning, expression, and purification of PfFn are provided as Supporting Information.

Temperature Stability Analysis of apo-PfFn. The apo-PfFn (3.36 mg/mL, 0.5 mL, 50 mM 4-(2-hydroxyethyl)-1-piperazineethanesulfonic acid (HEPES), 100 mM NaCl, pH 7.0) was incubated at 110 and 120 °C in an oil bath for 20 min. The protein solution was allowed to cool before being cleared by centrifugation (10 min at 12 100 × *g*). The cage assembly was assessed by dynamic light scattering (DLS, Brookhaven 90Plus Particle Size Analyzer) measured at 90° with a 661 nm diode laser, and the correlation function was fit using a non-negatively constrained least-squares analysis. The particle size and the amount of assembled protein,

(25) Yamashita, I.; Hayashi, J.; Hara, M. *Chem. Lett.* **2004**, *33*, 1158.
(26) Iwahori, K.; Yoshizawa, K.; Muraoka, M.; Yamashita, I. *Inorg. Chem.* **2005**, *44*, 6393.
(27) Iwahori, K.; Morioka, T.; Yamashita, I. *Phys. Status Solidi* **2006**, *203*, 2658.
(28) Douglas, T.; Strable, E.; Willits, D.; Aitouchen, A.; Libera, M.; Young, M. *Adv. Mater.* **2002**, *14*, 415.
(29) Douglas, T.; Young, M. *Nature* **1998**, *393*, 152.
(30) Douglas, T.; Young, M. J. *Science* **2006**, *312*, 873.
(31) Sun, J.; DuFort, C.; Daniel, M. C.; Murali, A.; Chen, C.; Gopinath, K.; Stein, B.; De, M.; Rotello, V. M.; Holzenburg, A.; Kao, C. C.; Dragnea, B. *Proc. Natl. Acad. Sci. U.S.A.* **2007**, *104*, 1354.
(32) Khalil, A. S.; Ferrer, J. M.; Brau, R. R.; Kottmann, S. T.; Noren, C. J.; Lang, M. J.; Belcher, A. M. *Proc. Natl. Acad. Sci. U.S.A.* **2007**, *104*, 4892.
(33) Hyeon, T.; Lee, S. S.; Park, J.; Chung, Y.; Na, H. B. *J. Am. Chem. Soc.* **2001**, *123*, 12798.
(34) Rockenberger, J.; Scher, E. C.; Alivisatos, P. *J. Am. Chem. Soc.* **1999**, *121*, 11595.
(35) Zeng, H.; Li, J.; Wang, Z. L.; Liu, J. P.; Sun, S. *Nano Lett.* **2004**, *4*, 187.
(36) Sun, S.; Zeng, H.; Robinson, D. B.; Raoux, S.; Rice, P. M.; Wang, S. X.; Li, G. *J. Am. Chem. Soc.* **2004**, *126*, 273.
(37) Tatur, J.; Hagedoorn, P. L.; Overeijnder, M. L.; Hagen, W. R. *Extremophiles* **2006**, *10*, 139.
(38) Reindel, S.; Schmidt, C. L.; Anemuller, S.; Matzanke, B. F. *Biochem. Soc. Trans.* **2002**, *30*, 713.
(39) Usui, K.; Ishii, N.; Kawarabayasi, Y.; Yohda, M. *Protein Sci.* **2004**, *13*, 134.
(40) Kim, R.; Kim, K. K.; Yokota, H.; Kim, S. H. *Proc. Natl. Acad. Sci. U.S.A.* **1998**, *95*, 9129.
(41) Wiedenheft, B.; Mosolf, J.; Willits, D. A.; Yeager, M.; Dryden, K. A.; Young, M. J.; Douglas, T. *Proc. Natl. Acad. Sci. U.S.A.* **2005**, *102*, 10551.
(42) Ramsay, B.; Wiedenheft, B.; Allen, M. A.; Gauss, G. H.; Lawrence, C. M.; Young, M. J.; Douglas, T. *J. Inorg. Biochem.* **2006**, *100*, 1061.
(43) Varpness, Z.; Peters, J. W.; Young, M.; Douglas, T. *Nano Lett.* **2005**, *5*, 2306.
(44) Matias, P. M.; Tatur, J.; Carrondo, M. A.; Hagen, W. R. *Acta Crystallogr., Sect. F* **2005**, *61*, 503.
(45) Tatur, J.; Hagen, W. R.; Matias, P. M. *J. Biol. Inorg. Chem.* **2007**, *12*, 615.

relative to an unheated sample, were independently estimated by chromatography on a Superose 6 size exclusion column run on an Amersham/Pharmacia Akta FPLC (GE Healthcare, Piscataway, NJ) equilibrated with 50 mM HEPES and 100 mM NaCl buffer at pH 7.0. The flow rate was 0.5 mL min^{-1}, and the elution of the protein was monitored at 260, 280, and 410 nm.

PfFn γ-Fe_3O_4 Mineralization. For reactions performed at 65 °C, 10 mL of a deaerated solution of 100 mM NaCl and 5 mg of PfFn protein (1.0×10^{-5} mmol) were added to an N_2-flushed jacketed glass centrifuge tube sealed with a rubber septum. For reactions performed at 85 °C, the volume of the deaerated salt solution was increased to 15 mL. The temperature of the reaction was maintained by circulating water through the jacket flask, and the reaction was brought to pH 8.5 using 50 mM sodium hydroxide (NaOH) with an automatic titrator (Brinkmann 718 AutoTitrator). Deaerated solutions of $(NH_4)_2Fe(SO_4)\cdot 6H_2O$ (12.5 mM, 0.821 mL) and H_2O_2 (2.5 mM, 0.821 mL) were added simultaneously and at a constant rate (0.055 mL min^{-1}) using a syringe pump (Kd Scientific, New Hope, PA). For an iron loading factor of 1000 Fe/cage, approximately 1.0×10^{-2} mmol of Fe^{2+} was added for 5 mg of the protein. For an iron loading factor of 2000 Fe/cage, approximately 2.1×10^{-2} mmol of Fe^{2+} was added for 5 mg of the protein. Solutions of H_2O_2 were freshly prepared, and the stock H_2O_2 concentration was determined spectrophotometrically.[46] The H^+ generated during the reaction was titrated dynamically with a Brinkmann 718 automatic titrator using 50 mM NaOH to maintain a constant pH of 8.5. Metal ion and oxidant solutions were added over 15 min during a 1000 Fe loading reaction, and the reaction was considered complete 15 min later. For a 2000 Fe loading reaction, the metal ion and oxidant solutions were added over 7.5 min to minimize bulk precipitate formation, and the reaction was considered complete 22 min later. After completion, the reaction was cooled on ice, and 1 mL of 0.3 M sodium citrate was added to chelate any free iron species. The reaction solution was then allowed to dialyze against 100 mM NaCl overnight.

Particle Characterization. DLS and Superose 6 size exclusion chromatography (SEC) were performed before and after mineralization to confirm the protein assembly and particle size as in the temperature stability analysis section. Protein particle size was also confirmed by transmission electron microscopy (TEM, Leo 912AB TEM, Oberkochen, Germany) operating at 100 keV with 2% uranyl acetate staining. γ-Fe_2O_3 particle size and electron diffraction data were collected on unstained mineralized PfFn samples, and *d* spacings calculated from the diffraction patterns were compared to the International Centre for Diffraction Data powder diffraction files for Fe_3O_4 (19-0629) and γ-Fe_2O_3 (39-1346) after calibration of the microscope with a Au standard. The samples were lyophilized to produce dehydrated particles for magnetic characterization. Alternating current magnetic susceptibility (ACMS) measurements were performed on the pellet using the alternating current magnetic susceptometer option of the Quantum Design Physical Properties Measurement System. The magnetic susceptibility was monitored at 100, 500, 1000, 5000, and 10 000 Hz with an oscillation amplitude of 10 G while being cooled from 125 K to 4 K. The average superparamagnetic blocking temperature (T_b) was determined at each frequency. These data were fit to the Néel−Arrhenius equation to determine the interaction behavior of the particles.[47] The magnetic response of the particles to an applied magnetic field was probed using vibrating sample magnetometry (VSM). Hysteresis of the particles was collected from 6 to −6 T at 5 K, and the coercive field (H_c) was extracted from the resulting loops.

Electrostatic Surface Calculation. The Protein Databank (PDB) structure files for horse spleen L-chain ferritin (1DAT), human H-chain ferritin (2FHA), and *P. furiosus* ferritin (2JD6) were obtained from the Protein Databank (www.rcsb.org/pdb/). Molecular images of the dimers of each ferritin as well as the *P. furiosus* half-cage were created from the PDB files using Chimera (University of California—San Francisco) and were saved as PDB files.[48] The electrostatic surface potential was calculated using Graphical Representation and Analysis of Structural Properties (GRASP) software installed on an SGI system.[49] The exterior and interior dielectric constants were set to 80.0 and 2.0, respectively.

Results and Discussion

PfFn has been shown to be stable at temperatures significantly higher than previously attainable with ferritins from a diverse spectrum of organisms.[37] The innate stability of PfFn makes it an excellent candidate for investigations of biological, chemical, and synthetic reactions at elevated temperatures. Here, the results of a synthetic investigation of γ-Fe_2O_3 synthesized at 65 and 85 °C using PfFn as a constrained biotemplate are reported. The physical and magnetic characteristics of the γ-Fe_2O_3 nanoparticles synthesized at 65 or 85 °C using this hyperthermophilic archaeal ferritin are compared to those previously seen with horse spleen (HsFn) and a mutant of human H-chain ferritin (referred to here as HFn).[18,24,50] Significantly, γ-Fe_2O_3 nanoparticles synthesized in PfFn exhibit a rapid magnetic saturation which occurs at a much lower field strength as compared to that of previously reported particles synthesized using HsFn or HFn (approximately 55% less for 1000 Fe/cage reaction products), suggesting that the PfFn derived particles are composed of single magnetic domains and exhibit square hysteresis reminiscent of thin films.

PfFn was heterologously expressed to high levels in *E. coli*, and upward of 90 mg of protein were obtained from purification of 4 L of liquid *E. coli* cultures. A 90 °C heat denaturation step followed by a rapid pH change from 7.0 to 4.0 and back by dialysis removed most of the *E. coli* proteins and cellular debris. SEC (Superose 6) yielded pure protein as confirmed by sodium dodecyl sulfate polyacrylamide gel electrophoresis (SDS-PAGE) analysis and mass spectrometry (Supporting Information Figure S1). The purified protein was compared to HsFn by SEC, DLS, and TEM analysis (Supporting Information Figure S2). Electron micrographs revealed that PfFn adopts the characteristic spherical cage-like architecture of ferritins with a diameter of approximately 12 nm, consistent with the crystal structure of PfFn and other ferritins (PfFn = 12 ± 0.97 nm, HsFn = 12 ± 1.2 nm).[44,45,51,52] DLS analysis confirmed the PfFn

(46) Hildebrandt, A. G.; Roots, I. *Arch. Biochem. Biophys.* **1975**, *171*, 385.
(47) Kilcoyne, S. H.; Cywinski, R. *J. Magn. Magn. Mater.* **1995**, *140*, 1466.
(48) Pettersen, E. F.; Goddard, T. D.; Huang, C. C.; Couch, G. S.; Greenblatt, D. M.; Meng, E. C.; Ferrin, T. C. *J. Comput. Chem.* **2004**, *25*, 1605.
(49) Nicholls, A.; Sharp, K. A.; Honig, B. *Struct. Funct. Genet.* **1991**, *11*, 281.
(50) Resnick, D.; Gilmore, K.; Idzerda, Y. U.; Klem, M. T.; Smith, E.; Douglas, T. *J. Appl. Phys.* **2004**, *99*, 7127.
(51) Gallois, B.; d'Estaintot, B. L.; Michaux, M. A.; Dautant, A.; Granier, T.; Precigoux, G.; Soruco, J. A.; Roland, F.; Chavas-Alba, O.; Herbas, A.; Crichton, R. R. *J. Biol. Inorg. Chem.* **1997**, *2*, 360.
(52) Hempstead, P. D.; Yewdall, S. J.; Fernie, A. R.; Lawson, D. M.; Artymiuk, P. J.; Rice, D. W.; Ford, G. C.; Harrison, P. M. *J. Mol. Biol.* **1997**, *268*, 424.

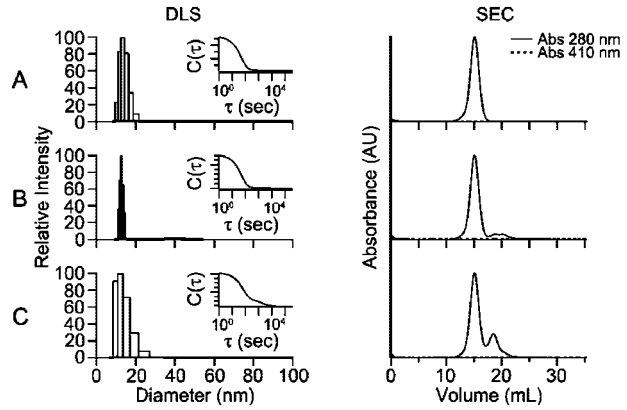

Figure 1. Temperature stability of PfFn. (A) Unheated control, (B) 110 °C, and (C) 120 °C incubated samples were analyzed by DLS and SEC to determine the remaining amount of protein and the state of assembly. The incubated samples remained assembled with the correct cage diameter, and most of the protein remained soluble as indicated by the integrated peak areas from SEC. The narrower DLS distribution of B is a result of the error of the analytical technique (±2% signal intensity).

diameter (mean = 12 ± 1.1 nm) in comparison to that of HsFn (mean = 12 ± 1.2 nm) as well as revealed that the cages are monodisperse in solution. A similar retention on SEC confirmed that the PfFn and HsFn are approximately the same size (HsFn = 15.64 mL, PfFn = 15.86 mL).

The temperature range in which PfFn remained stable and assembled was determined to optimize the desired γ-Fe_2O_3 synthesis. The protein was verified to be stable to temperatures up to 120 °C by heating the purified PfFn to 110 or 120 °C for 20 min in a Parr bomb. The resulting solution was analyzed by DLS and SEC for cage assembly and aggregation (Figure 1). DLS revealed that PfFn remained assembled and monodisperse (unheated sample diam = 12 ± 1.1 nm, 110 °C sample = 12 ± 0.04 nm, 120 °C sample = 11 ± 0.66 nm). The integration of the elution profile from the SEC (Superose 6) was used to quantitate the amount of PfFn that remained intact. The elution profiles showed near identical retention (unheated sample = 15.10 mL, 110 °C sample = 15.12 mL, 120 °C sample = 15.10 mL; Figure 1), and integrating the peaks revealed that 96% of the total protein remained in solution after 110 °C incubation with 91% remaining intact as an assembled cage. After 120 °C incubation, 91% of the total protein remained soluble, with 73% remaining intact as an assembled cage. These data confirmed the potential utility of PfFn as a template for high temperature inorganic synthesis of γ-Fe_2O_3.

The synthesis of ferrimagnetic γ-Fe_2O_3 templated by the apo-PfFn and HsFn cages was performed under conditions of elevated pH, temperature, and controlled oxidation. The reactions were performed using two stoichiometric loading factors of 1000 or 2000 Fe/cage. All reactions yielded homogeneous brown solutions. The incorporation of iron into the cage could be easily distinguished from the bulk precipitation by light scattering and centrifugation, and reactions run in the absence of ferritin cages resulted in the precipitation of bulk iron oxide from solution as reported previously.[24,53] As previously described, HsFn successfully

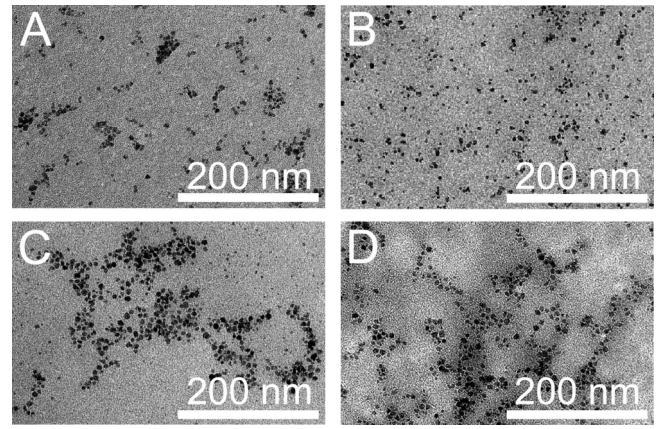

Figure 2. Unstained TEM images of PfFn-encapsulated γ-Fe_2O_3 nanoparticles synthesized under different temperatures and different Fe^{2+} loading factors. (A) 65 °C, 1000 Fe/cage; (B) 85 °C, 1000 Fe/cage; (C) 65 °C, 2000 Fe/cage; and (D) 85 °C, 2000 Fe/cage.

Table 1. Measured Physical and Magnetic Characteristics of PfFn-Encapsulated γ-Fe_2O_3 Nanoparticles and Previously Reported Characteristics of HFn- and HsFn-Encapsulated γ-Fe_2O_3 Nanoparticles[24,47]

PfFn-Encapsulated γ-Fe_2O_3			
TEM particle diameter (nm)	DLS cage diameter (nm)	T_b (K)	H_c (G)
	65 °C, 1000 Fe/Cage		
4.5 ± 1.3	12 ± 0.68	10 ± 0.04	126.17 ± 7.03
	85 °C, 1000 Fe/Cage		
4.0 ± 1.1	12 ± 1.6	8.7 ± 0.22	60.95 ± 0.47
	65 °C, 2000 Fe/Cage		
6.9 ± 1.2	12 ± 1.4	34 ± 0.14	249.95 ± 1.10
	85 °C, 2000 Fe/Cage		
5.8 ± 1.2	13 ± 2.8	36 ± 0.09	259.83 ± 27.4

Mammalian Ferritin-Encapsulated γ-Fe_2O_3			
sample	TEM particle diameter (nm)	T_b (K)	H_c (G)
HsFn, 65 °C, 1000 Fe/cage	5.9 ± 1.3	17.5	176.90 ± 4.44
HFn, 65 °C, 1000 Fe/cage	3.8 ± 0.7	11	754.99 ± 4.76
HFn, 65 °C, 3000 Fe/cage	5.5 ± 0.9	27	567.71 ± 11.8
HFn, 65 °C, 5000 Fe/cage	6.0 ± 0.9	36	650.95 ± 11.7

formed protein encapsulated minerals at temperatures up to 65 °C, but introduction of HsFn to an 85 °C vessel resulted in the precipitation of the protein from the solution and the formation of bulk iron oxide (data not shown). In contrast, PfFn was able to successfully template the reaction under both 1000 Fe/cage and 2000 Fe/cage loading factor conditions at both 65 and 85 °C. Reactions performed at temperatures higher than 85 °C resulted in the formation of bulk iron oxides (data not shown), possibly as a result of the heterogeneous nucleation on the small amount of denatured protein.

Physical characterization of the reaction products by TEM, SEC, and DLS revealed significant differences between the 65 and 85 °C γ-Fe_2O_3 nanoparticles. Observation of the reaction product by TEM showed electron-dense nanoparticles (Figure 2) with particle size differences that were sensitive to both the loading factor and the temperature (Table 1). In general, γ-Fe_2O_3 particles synthesized at 85 °C had smaller average particle diameters that those seen at 65 °C, and reactions performed under the 2000 Fe/cage

(53) Strable, E.; Bulte, J. W. M.; Moskowitz, B.; Vivekanandan, K.; Allen, M. A.; Douglas, T. *Chem. Mater.* **2001**, *13*, 2201.

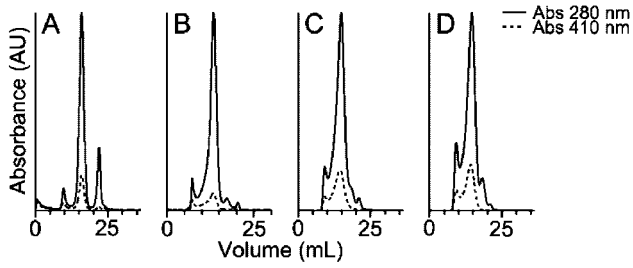

Figure 3. SEC of PfFn after γ-Fe_2O_3 synthesis. (A) 65 °C synthesis with a 1000 Fe/cage loading factor, (B) 85 °C synthesis with a 1000 Fe/cage loading factor, (C) 65 °C synthesis with a 2000 Fe/cage loading factor, and (D) 85 °C synthesis with a 2000 Fe/cage loading factor. Monitoring elution at both 280 and 410 nm shows coelution of the PfFn with the synthesized mineral (central peak), which was easily isolated from the bulk material (early peak) and the degradation products (late peak).

loading conditions yielded larger particles than those under the 1000 Fe/cage conditions. Negatively stained samples (2% uranyl acetate) revealed the intact protein cage, with γ-Fe_2O_3 formation having occurred inside the cages (Supporting Information Figure S3). Electron diffraction resulted in a pattern consistent with γ-Fe_2O_3 (Supporting Information Figure S4). DLS showed that the PfFn particles remained intact with diameters as indicated in Table 1. SEC of the protein monitored at 280 nm (protein absorbance) and 410 nm (mineral absorbance) showed coelution of the mineral with the protein cage, confirming that the mineral nucleated and grew on the inside of the ferritin cages (Figure 3). These data show that the protein mediated synthesis of γ-Fe_2O_3 nanoparticles is spatially confined to the interior of the ferritin protein cage.

Magnetic characterization of the PfFn-encapsulated γ-Fe_2O_3 nanoparticles revealed a significant enhancement of the magnetic hysteresis as compared to that of previously synthesized particles with protein cage templates.[18,54] The PfFn-templated particles displayed a rapid magnetic saturation at low magnetic field strengths (2.0–4.4 T). The response of the particles to a magnetic field was probed at 5 K by reversibly scanning from 6 to −6 T to generate the hysteresis loops shown in Figure 4. The loops exhibited square hysteresis with small coercive fields (H_c) reminiscent of ordered magnetite thin film behavior in that these materials saturated at lower magnetic field strengths (<2 T). This behavior is very different from previous observations of γ-Fe_2O_3 synthesized in HsFn and HFn, which showed saturation at fields of 6 T or greater.[18,24] A comparison of the hysteresis loops of γ-Fe_2O_3 synthesized in HsFn, HFn, and PfFn is shown in Figure 4. This behavior was observed under all loading conditions and synthetic temperatures. The saturation behavior of the PfFn-encapsulated nanoparticles is consistent with a single magnetic domain particle, whereas the HsFn and HFn derived particles behave like multidomain particles or single domains of varying size and strength. While each HsFn- or HFn-derived particle is a single domain, the ensemble is composed of various sized magnetic domains. In contrast, a single domain particle of γ-Fe_2O_3 in PfFn exhibited a characteristic field strength at which the spins flip in a concerted manner, resulting in the sharper transition.

The VSM studies also revealed significant differences in the coercive fields (H_c) for the PfFn-encapsulated magnetite nanoparticles as compared to HsFn and HFn. H_c of the PfFn-derived particles shows the expected size dependent behavioral response to an external magnetic field (Table 1). γ-Fe_2O_3 particles synthesized in PfFn under the 1000 Fe/cage conditions showed variability dependent on the synthesis temperature (65 °C reaction product = 126.17 G vs 85 °C reaction product = 60.95 G) and displayed less than half the field strength of that of the particles synthesized under the 2000 Fe/cage conditions. In contrast, the variability of H_c in the 2000 Fe/cage PfFn was lower (65 °C, 249.95 G; 85 °C, 259.83 G). The differences between H_c for loading conditions at both 65 and 85 °C followed the expected size effects: smaller particles have a smaller H_c. Comparing the 1000 Fe/cage PfFn, HsFn, and HFn encapsulated γ-Fe_2O_3 particles revealed that the H_c for the PfFn-derived particles was significantly smaller than for either HsFn or HFn (Table 1).

Further magnetic characterization of the PfFn-encapsulated γ-Fe_2O_3 nanoparticles by ACMS revealed properties nearly identical to those seen with other ferritins. The mineralized cages were analyzed over a temperature range of 4–125 K under a 10 G oscillating magnetic field to analyze the ferrimagnetic blocking temperature (T_b) of the protein−mineral composites.[55] The T_b was observed to be strongly dependent

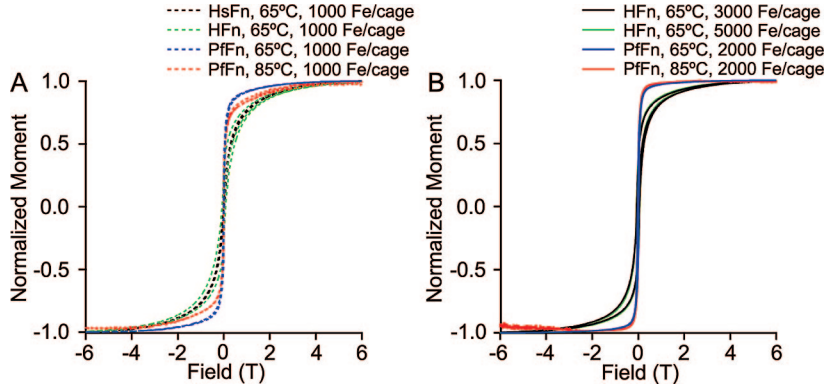

Figure 4. Comparison of hysteresis loops of PfFn-, HFn-, and HsFn-encapsulated γ-Fe_2O_3 nanoparticles. (A) Loops for 1000 Fe/cage loading of all three different ferritins. The PfFn-encapsulated particles show a significant decrease of field strength required to saturate the particles and are reminiscent of magnetic thin films. (B) Loops for higher loading factors for PfFn and HsFn. The rapid saturation of the PfFn-encapsulated nanoparticles is markedly apparent.

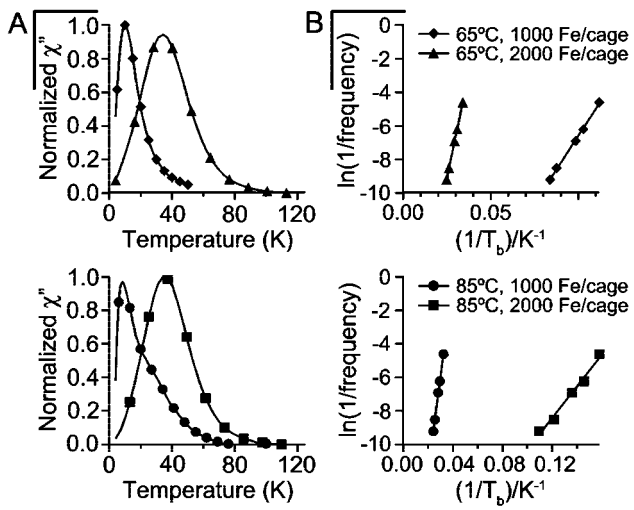

Figure 5. (A) ACMS measurements of mineralized PfFn at 1000 Hz under a 10 G magnetic field under the two loading factors tested. (B) Néel−Arrhenius fits of the ACMS data. The linearity of the data indicates that the particles are not interacting.[47]

on the particle size of the encapsulated γ-Fe_2O_3. For the 1000 Fe/cage PfFn, the T_b varied between 7–13 K whereas for the 2000 Fe/cage products it varied between 30–35 K (Figure 5, Table 1). No significant enhancements of T_b were observed for reactions performed at 85 °C at either loading factor when compared to the 65 °C syntheses with PfFn, HsFn, and HFn.[24,47] The magnetic susceptibility of the minerals was probed at different frequencies, and $\ln(1/f)$ versus $1/T_b$ was plotted, where f is the measurement frequency. The data were then fit according to the Néel−Arrhenius equation (eq 1) to analyze the interactions between the particles.[47]

$$\ln(1/f) = \ln(\tau_0) + (E_a/k_B)(1/T_b) \quad (1)$$

All synthesized materials exhibited linear Néel−Arrhenius relationships, indicating that the particles are magnetically isolated and noninteracting presumably as a result of the separation afforded by the protein coat around each particle.[47]

The magnetic behavior observed for the PfFn templated γ-Fe_2O_3 was significantly different from the syntheses performed within HsFn and HFn but not significantly affected by the reaction temperature up to 85 °C. Therefore, the unusual magnetic behavior may be due to some intrinsic feature of the protein template itself. It is possible that PfFn exhibits different biochemical properties of the interior of the cage, compared to HsFn and HFn, that are responsible for the properties of the synthetic γ-Fe_2O_3. We compared the protein crystal structures of *P. furiosus* (PDB: 2JD6), horse spleen L-chain (PDB: 1DAT), and human H-chain (PDB: 2FHA) ferritin, specifically at the purported nucleation sites located at the 2-fold axis on the interior surface of the cage. Mapping out the acidic residues exposed on the interior surface showed a significant difference in the nucleation sites between the archaeal and the mammalian ferritins. Previous studies have shown that the residues Glu53, Glu56, Glu57, and Glu60 (horse spleen L-chain) and Glu61 and Glu64 (human H-chain) are responsible for the nucleation of the iron oxide mineral.[56] These residues are clustered in a small patch on the 2-fold axis in a semicircular area (Figure 6). However, the structure of the interior of the *P. furiosus* ferritin is significantly different. The partially resolved hydrophobic C-terminal ends of the PfFn subunits cross over the 2-fold axis above the surface where the mammalian nucleation sites would be located. An acidic patch is located

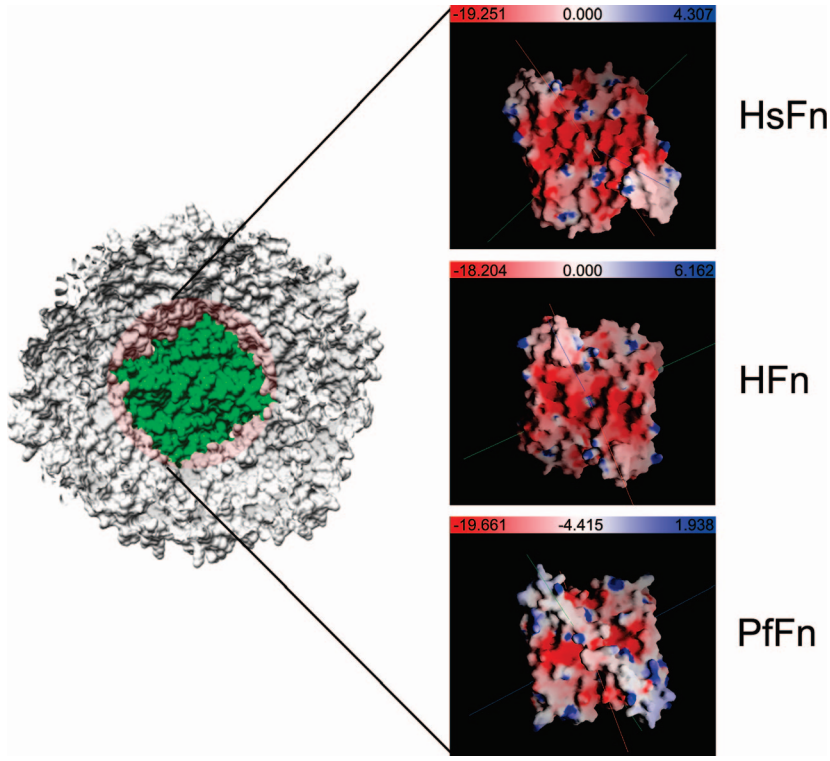

Figure 6. Colored visualization of the electrostatic potentials of HsFn, HFn, and PfFn. Red indicates negative charge, blue indicates positive charge, and white indicates charge neutral areas. The hydrophobic C-terminus of the PfFn lies over the identified nucleation sites in other ferritins, possibly limiting nucleation on the interior cage surface.

away from the 2-fold axis and could provide a site for the nucleation to occur. However, this acidic patch contains fewer acidic amino acid residues as compared to the mammalian ferritins. Furthermore, it is possible that the C-terminus is quite floppy and may block these potential nucleation sites. We speculate therefore that if fewer nucleation sites in PfFn are exposed, the single domain γ-Fe_2O_3 particles could be formed from a single nucleation event occurring in the hollow space inside the PfFn cage without any protein scaffold to direct the mineral formation. Exposed nucleation sites would produce multiple nucleation events, and the growth of these distinct crystals into a single particle could result in the formation of multiple domain γ-Fe_2O_3 particles.

Conclusions

In this study, we highlighted the use of a thermostable ferritin from the hyperthermophilic archaeon *P. furiosus* in the synthesis of maghemite nanoparticles with potential applications in MRI, hyperthermia treatment, and magnetic memory storage. The protein cage template was shown to be stable at temperatures up to 120 °C. PfFn was able to successfully template the nanoparticles while maintaining its cage-like architecture. The particles exhibited distinctly different magnetic saturation from those seen in mammalian ferritin−mineral composites. In investigating reasons for this difference, we discovered that the electrostatic potential of the interior of the *P. furiosus* ferritin is markedly different from that of the mammalian ferritins and may be responsible for the differences in iron oxide nucleation, which has a significant effect on the observed magnetic properties.

(54) Meldrum, F. C.; Heywood, B. R.; Mann, S. *Science* **1992**, *257*, 522.
(55) Moskowitz, B. M.; Frankel, R. B.; Walton, S. A.; Dickson, D. P. E.; Wong, K. K. W.; Douglas, T.; Mann, S. *J. Geophys. Res.* **1997**, *102*, 22671.
(56) Chasteen, N. D.; Harrison, P. M. *J. Struct. Biol.* **1999**, *126*, 182.

This study confirms the utility of using thermostable protein templates for high temperature inorganic synthetic reactions. Thermostable enzymes (such as taq polymerase) have already revolutionized the field of biotechnology, so it is likely that templates with the same robustness will also lead to innovations in material science and materials engineering. Materials exhibit novel and interesting properties when synthesized on the nanoscale, but these syntheses usually have been restricted to solvent based methods of synthesis because of the instability of the biological templates. The use of temperature stable biological templates will add distinct advantages to the utility of these materials in industry and medicine. Biomolecular templates are potentially available in a variety of shapes and sizes, and the ability also to modify the template interfaces and exterior surfaces can be used to introduce targeting for delivery or scaffolding for higher structure synthesis. As such, PfFn highlights one of a possible variety of temperature stable templates that will potentially revolutionize materials synthesis and science.

Acknowledgment. We would like to thank Sue Brumfield for help with the electron microscopy. This work was supported in part by the MSU NCUR/Lancy Program, CBS Program (NIH Grant GM62423-02), Beckman Scholars Program (M.J.P.), and the Air Force Office of Scientific Research (FA9550-07-1-533).

Supporting Information Available: Cloning, expression, and purification of the *P. furiosus* ferritin. Morphological comparisons between horse spleen ferritin and *P. furiosus* ferritin as well as molecular weight confirmations by SDS-PAGE and mass spectrometry. Electron diffraction data confirming the identity of the iron oxides synthesized in *P. furiosus* ferritin (PDF). This material is available free of charge via the Internet at http://pubs.acs.org.

CM702732X